Local cusp solutions of viscous flow

R. Brandão[1], J. Eggers[1]†, M. A. Fontelos[2]

[1]School of Mathematics, University of Bristol, Fry Building, Woodland Road, Bristol BS8 1UG, United Kingdom
[2] Instituto de Ciencias Matemáticas, (ICMAT, CSIC-UAM-UCM-UC3M), C/ Serrano 123, 28006 Madrid, Spain

(Received xx; revised xx; accepted xx)

Free surface cusps are a generic feature of externally driven, viscous flow bounded by a free surface. Here we present an alternative to the boundary integral description found recently [J. Eggers, Phys. Rev. Fluids **8**, 124001 (2023)], which instead is based directly on a local analysis of the Stokes equation. The new description has the advantage of greater simplicity and transparency, making it easier to generalize to more complex solutions with several parameters.

1. Introduction

When a viscous fluid with a free surface is strongly driven, the free surface is often seen to deform into a cusp singularity, rounded at the tip on a small scale only. As long as the driving varies slowly in the third dimension, the tip position is close to a straight line, and the flow can be regarded as effectively two-dimensional. The formation of free-surface cusps was first highlighted and demonstrated experimentally by Joseph *et al.* (1991), placing two counter-rotating rollers beneath the free surface of a viscous fluid, dragging fluid into the space between them. The observed cusps were so sharp that it lead Joseph *et al.* (1991) to propose that the free surface was indeed ending in a point, producing a non-differentiable surface even in the presence of surface tension.

To investigate this question, Jeong & Moffatt (1992) constructed an exact solution to the two-dimensional viscous flow equations, driven by a vortex dipole underneath a free surface, using the method of complex mapping from the unit disk unto the flow domain. They found that the tip size remains finite, but is exponentially small in the capillary number, which is the flow speed, made dimensionless using the capillary speed γ/η. Here γ is the coefficient of surface tension between the liquid and an inert exterior gas, and η is the shear viscosity of the liquid. This exponential dependence was later verified experimentally by Lorenceau *et al.* (2003), using an apparatus similar to that used by Joseph *et al.* (1991) and Jeong & Moffatt (1992).

Cusps play an important role in free surface flow, because they provide a key mechanism for the entrainment of air into a liquid bath (Kiger & Duncan 2012). Owing to the exponential shrinkage of the tip size with capillary number, the gap inside the cusp becomes extremely narrow. This means that an external fluid (such as air), which is drawn into the cusp, produces an elevated lubrication pressure inside the narrow gap, which eventually leads to a bifurcation (Eggers 2001; Lorenceau *et al.* 2004), even if the viscosity of the outer liquid is much smaller than that of the bath. As a result of the bifurcation, a sheet of air is drawn into the liquid (Lorenceau *et al.* 2004), opening a channel for air entrainment. In the present paper, however, we will disregard the effect of

† Email address for correspondence: jens.eggers@bristol.ac.uk

any external fluid, and focus on the formation of the cusp and its relation to the driving flow.

Following Jeong & Moffatt (1992), many more exact two-dimensional solutions similar to that of Jeong & Moffatt (1992) were constructed using the method introduced by Richardson (1968), placing various singularities underneath a flat surface (Jeong & Moffatt 1992; Jeong 2010, 1999, 2007), or near a two-dimensional "bubble" (Antanovskii 1996; Crowdy 2002; Cummings & Howison 1999; Cummings 2000). The existence of these solutions suggests that cusp formation is a generic phenomenon for viscous flow with a free surface, and that cusp solutions can be understood by a local argument, independent of a particular driving flow. Solutions should moreover be robust against small three-dimensional perturbations.

The problem of finding local cusp solutions has recently been addressed by one of us (Eggers 2023), using a boundary integral method. However, the necessary calculations are quite involved, and the integral formulation obscures the simple force balance expressed by the equations of fluid motion. Instead, here we pursue an alternative approach proposed in Howison *et al.* (1997); Morgan (1994); Gillow (1998), which relies on a direct solution of the Stokes equation, but simplified on account of the slenderness of the cusp.

In the following, we assume that all lengths have been made dimensionless using some external length scale L, which is a feature of the particular geometry of the apparatus at hand. In the example of Jeong & Moffatt (1992)'s solution, in which the flow is driven by a vortex dipole underneath a free surface, this could be the depth of the dipole in its rest state of vanishing dipole strength. Velocities are measured in units of the capillary speed γ/η, so that $\eta L/\gamma$ is a time scale. We are solving the two-dimensional, steady, viscous flow equations with a free surface, written as $y = h(x)$, and assuming symmetry about the x-axis, see Fig. 1. The viscous flow equation in the bulk is

$$\boldsymbol{\nabla} p = \triangle \mathbf{v}, \tag{1.1}$$

where $\mathbf{v} = (u, v)$ is a two-dimensional velocity field, and p the pressure. On the free surface ($\boldsymbol{\sigma}$ the stress tensor) the stress boundary condition reads:

$$\mathbf{n} \cdot \boldsymbol{\sigma} = \frac{h''}{(1 + h'^2)^{3/2}} \mathbf{n}, \tag{1.2}$$

where a prime denotes the derivative with respect to the argument, and $\mathbf{n}$ is the normal to the free surface. The condition for a steady flow is

$$h' = \frac{v}{u}. \tag{1.3}$$

Equations (1.1)-(1.3) have been made dimensionless using the length L, time scale $\eta L/\gamma$, and pressure scale γ/L. We aim to solve (1.1)-(1.3) in the limit that the radius of curvature of the tip r_c (see Fig. 1) tends to zero.

2. Asymptotic solution

Our solution proceeds by matching two asymptotic regions shown schematically in Fig. 2 below. The tip region plays the role of an inner solution, the cusp region is the outer solution. We begin by describing both regions individually, and then show in more detail how they are matched.

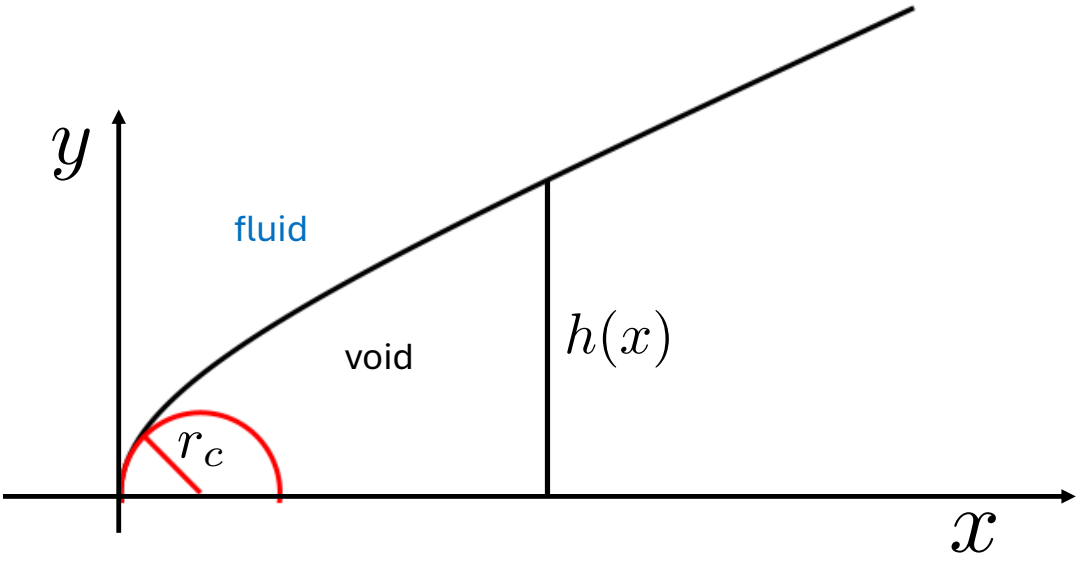

FIGURE 1. A sketch of the cusp geometry, symmetric about the x-axis: the shape is described by $h(x)$, there is a viscous fluid outside, the inside of the cusp contains a gas which does not exert any stress. The tip of the cups is rounded, with r_c the radius of curvature.

2.1. *The tip region*

The tip region has the form of a parabola $h = \sqrt{2r_c}x^{1/2}$, where r_c is the radius of curvature. This shape, together with an appropriate velocity field, is an exact steady solution of Stokes' equation with surface tension (Hopper 1993). This can be shown by solving the equations using the mapping

$$z = 2r_c w(\zeta) \equiv 2r_c\left(\zeta^2 + i\zeta\right), \tag{2.1}$$

where ζ real corresponds to the free surface. Thus the upper half of the ζ-plane is mapped unto the fluid domain, which is the outside of the cusp. In the Goursat representation (Jeong & Moffatt 1992), the stream function of the flow is written in terms of two holomorphic functions f and g:

$$\psi = \Im\left\{f(z) + \bar{z}g(z)\right\}; \tag{2.2}$$

the components of the velocity field are calculated from $u = \psi_y$ and $v = -\psi_x$, where the subscript denotes the derivative. However, in the complex formulation the velocity field is recovered more conveniently from

$$u - iv = f'(z) + \bar{z}g'(z) - \overline{g(z)}. \tag{2.3}$$

As shown in Hopper (1993), the steady flow around the parabola (2.1) is given by

$$f = \frac{i}{2}w'(\zeta)\bar{w}(\zeta)G(\zeta), \quad g = -\frac{i}{2}w'(\zeta)G(\zeta), \tag{2.4}$$

where

$$G = \frac{1}{2\pi i\sqrt{1+4\zeta^2}}\ln\left(\frac{2\zeta - \sqrt{1+4\zeta^2}}{2\zeta + \sqrt{1+4\zeta^2}}\right).$$

The free surface can be parameterized by putting $\zeta = \phi/2$, with ϕ real, the tangent vector to the parabola is $\mathbf{t} = (\phi, 1)/\sqrt{1+\phi^2}$, and thus the tangential velocity u_0 is found

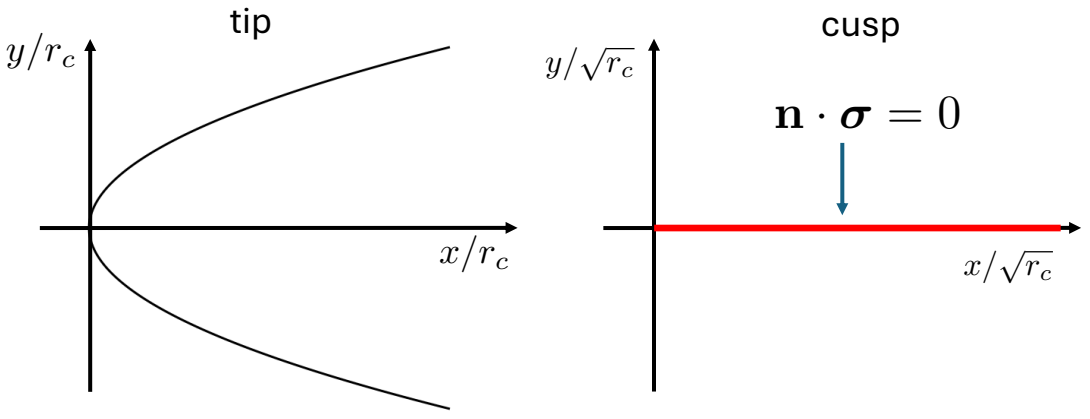

FIGURE 2. The inner (tip) region, which has typical scale r_c, is shown on the left; the interface reduces to a parabola in the limit $r_c \to 0$. In the outer (cusp) region, shown on the right, the interface reduces to the positive x-axis when viewed on scale $\sqrt{r_c}$, with $r_c \to 0$.

from $u_0 = (u\phi + v)/\sqrt{1+\phi^2}$. Using the solution (2.4), this gives

$$u_0(\phi) = -\frac{1}{\pi}\ln\left(\sqrt{1+\phi^2}+\phi\right), \quad \phi = \sqrt{2x/r_c}, \tag{2.5}$$

in agreement with Eggers (2023); the velocity near the interface can be inferred from

$$(u, v) = \frac{(1, h')}{\sqrt{1+h'^2}}u_0.$$

In the far field, along the interface

$$u_0 = -\frac{1}{2\pi}\ln\frac{8x}{r_c}, \tag{2.6}$$

which is the far field of a stokeslet, i.e. the velocity field generated by a point force of strength 2. This corresponds to each side of the interface pulling with force γ (per unit length in the third direction). Since $h' = \sqrt{r_c/(2x)}$, which vanishes for $x \to \infty$, we have

$$u = -\frac{1}{2\pi}\ln\frac{8x}{r_c}, \quad v = -\frac{\sqrt{r_c}}{2^{3/2}\pi\sqrt{x}}\ln\frac{8x}{r_c}, \tag{2.7}$$

again for large x.

2.2. *The cusp region*

In the cusp region, we can make use of slenderness and model the air gap as a cut in the complex plane along the positive x-axis, as illustrated in Fig. 2 b; this will be confirmed more formally below. We are seeking solutions to the Stokes equation symmetric about the x-axis and with stress-free conditions along the positive x-axis, valid locally around the tip of the cusp, which is at the origin. This is justified by the crucial observation that the stokeslet solution does not contribute to the stress at leading order, as we will see below.

Since the asymptotic problem of a cut of vanishing thickness is lacking a characteristic length scale, we seek power-law solutions for the stream function of the form (Eggers & Fontelos 2015)

$$\psi = r^\lambda\left[A\sin(\lambda\varphi) + C\sin((\lambda-2)\varphi)\right], \tag{2.8}$$

where r is the distance from the tip, and φ the angle measured from the negative x-axis. This ensures that the line $\varphi = 0$ in the wake of the cusp is a streamline, while the surface of the cusp is at $\varphi = \pi$. As shown in detail in Eggers & Fontelos (2015), eliminating the pressure and demanding that the two components of the normal stress vanish at the free surface $\varphi = \pi$, leads to the conditions $\sin \lambda\pi = 0$ or $\cos \lambda\pi = 0$ for the scaling exponent λ.

The first class of solutions leads to integer λ, with vanishing transversal velocity $v = 0$ along the cusp surface $x > 0$. Non-singular velocity fields correspond to $\lambda = 1, 2, \ldots$, yielding $u = x^n$, $n = 0, 1, \ldots$ for the tangential velocity along the cusp surface. Thus with $-U$ being the leading-order velocity sweeping past the cusp, a general superposition of these solutions yields the tangential velocity

$$u = -U + b_1 x + b_2 x^2 + \ldots, \tag{2.9}$$

with b_i being parameters. On the other hand, the second condition (and avoiding solutions too singular to match to the parabolic solution (2.4)), leads to $\lambda = 1/2, 3/2, \ldots$. Then on the positive x-axis, the velocity corresponding to these values is normal to the cusp, so that up to normalization $u = 0$, $v = \pm x^{(2n-1)/2}$, $n = 0, 1, 2, \ldots$, above and below the gap, respectively. This means a general superposition of normal velocities is of the form

$$u = 0, \quad v = a_0 x^{-1/2} + a_1 x^{1/2} + \ldots, \tag{2.10}$$

once more with a_i as free parameters.

Notice that in the special case $\lambda = 1$, the solution (2.8) becomes degenerate, and both terms lead to the same function. However, the "missing" solution can be found by putting $\lambda = 1 + \epsilon$, and letting $\epsilon \to 0$. Then at leading order one recovers the previous solution $\psi = r \sin \varphi = y$, while at order ϵ and putting $C = -A$ one obtains a new solution to Stokes' equation in the presence of a gap: $\psi = r \ln r \sin \varphi = y \ln r$, which is known as a stokeslet (Pozrikidis 1992). It describes the flow generated by a point force of strength unity, pulling in the positive x-direction, whose stream function is

$$\psi = -\frac{y}{4\pi} \ln(r/a), \tag{2.11}$$

where a is a positive constant. The solution (2.11) is distinct from (2.9) and (2.10), in that it breaks scale invariance.

As noted above, both components of the normal stress generated by (2.11) vanish on the surface $y = 0$. Now the velocity on the positive x-axis corresponding to (2.11) is $u = -\ln(x/a)/(4\pi)$ and $v = 0$, which matches (2.7) for a stokeslet of strength 2, and putting $a = r_c/8$. This means the total tangential component of the velocity is of the form

$$u = -\frac{1}{2\pi} \ln\left(\frac{8x}{r_c}\right) + b_1 x + b_2 x^2 + \ldots. \tag{2.12}$$

The leading-order contribution to (2.10) for which v remains finite at $x = 0$ is $a_1 x^{1/2}$; this is the one considered in Joseph *et al.* (1991); Eggers & Fontelos (2015). Together with a constant down-streaming $u = -U$ (which is the leading contribution to (2.9)), this produces a cusp which opens with a 2/3 exponent. The crucial new observation is that in order to match to the parabolic solution, we also have to add $a_0 x^{-1/2}$ to obtain

$$u = -U + b_1 x, \quad v = a_0 x^{-1/2} + a_1 x^{1/2}, \tag{2.13}$$

with higher order terms discarded.

Then since the interface is a streamline in steady state, we obtain for the slope

$$h' = \frac{v}{u} = -\frac{a_0}{U}x^{-1/2} - \left(\frac{a_1}{U} - \frac{a_0 b_1}{U^2}\right)x^{1/2} + O(x^{3/2}). \tag{2.14}$$

Thus identifying

$$r_c = 2\left(\frac{a_0}{U}\right)^2, \quad c = -\frac{2a_1}{3U} + \frac{a_0 b_1}{U^2}, \tag{2.15}$$

and integrating (2.14), this yields

$$h = \sqrt{2r_c}x^{1/2} + cx^{3/2}, \tag{2.16}$$

which is precisely the self-similar cusp profile found originally by Jeong & Moffatt (1992). Again, higher order terms have been discarded in order to obtain the leading order shape valid near the cusp tip. This is the central result of this paper, in which the structure of the cusp is obtained by local analysis of the flow equations alone.

For small x, (2.16) agrees with the parabolic solution (2.1). On the other hand, to leading order as $r_c \to 0$, comparing (2.12) and (2.9) provides the down-streaming velocity $U > 0$:

$$U = -\frac{1}{2\pi}\ln\frac{r_c}{8}, \tag{2.17}$$

which reveals an exponential dependence of the tip curvature on the externally imposed flow, as found originally by Jeong & Moffatt (1992).

2.3. *Matching*

We now make sure that the solution proposed above is consistent in the limit $r_c \to 0$, and that the different parts match. From (2.16) we see that the two terms on the right are balanced for $x = O(r_c^{1/2})$, so that both terms are of order $O(r_c^{3/4})$. For x on the order of r_c, we are in the tip region, conversely for x on the scale of $\sqrt{r_c}$, we are in the cusp region, as shown in Fig. 2. It follows that (2.16) can be written in self-similar form as

$$y = r_c^{3/4}H(x/r_c^{1/2}), \quad H(\xi) = (2\xi)^{1/2} + c\xi^{3/2}, \tag{2.18}$$

where c remains a free parameter, which depends on the particular problem at hand.

The structure of the matching problem is illustrated in Fig. 2. On the left, we show the inner, tip problem, which lives on scale r_c. It represents an exact solution to Stokes' equation with a free surface, which happens to be a parabola. Putting $\bar{x} = x/r_c$ and $\bar{y} = y/r_c$, this free surface can be written as

$$\bar{y} = \sqrt{2\bar{x}}. \tag{2.19}$$

On the right of Fig. 2, we illustrate the outer, cusp solution on scale $\sqrt{r_c}$. It follows from (2.18) that in the limit $r_c \to 0$ the surface degenerates to a line, occupying the positive x-axis, shown as the thick red line. Moreover, we now show that to leading order the boundary condition on the cut is stress free, as assumed in deriving solutions (2.9)-(2.11). First, using the scaling (2.18), we estimate the curvature in (1.2) as $\kappa = O(r_c^{3/4}/\sqrt{r_c}^2) = O(r_c^{-1/4})$. Second, to estimate the stress, we note that the stokeslet solution (2.11), for which $v = 0$, does not contribute to the stress. At next order, combining (2.13) and (2.15), we have $v \approx a_0 x^{-1/2} = O(\sqrt{r_c/x}\ln r_c)$. Estimating the derivative at scale $\sqrt{r_c}$, we find

$$\sigma = O(\sqrt{r_c/x^3}\ln r_c) = O(r_c^{-1/4}\ln r_c), \tag{2.20}$$

which dominates the curvature by a logarithmic factor, and justifies looking for stress-free cusp solutions.

Finally, we confirm the matching between the inner and outer velocity fields by comparing the outer limit of the inner solution to the inner limit of the outer solution. In the limit $r_c \to 0$,we find from (2.7) (the inner solution):

$$u = \frac{1}{2\pi} \ln \frac{r_c}{8} = -U, \quad v = \frac{\sqrt{r_c}}{2^{3/2}\pi\sqrt{x}} \ln \frac{r_c}{8} = \sqrt{\frac{r_c}{2x}} U, \tag{2.21}$$

using (2.17). If one considers the inner limit of (2.10), one obtains $v = a_1 x^{-1/2} = \sqrt{r_c/2} U x^{-1/2}$, which is the second equation of (2.21), which demonstrates the required matching.

2.4. *The outer flow*

The flow defined by (2.12) has the property that it is not bounded at infinity, so one might worry that it cannot be matched to a finite outer flow. We will now show that this is not a limitation of the present approach. Rather, solutions of the form (2.9) can be superimposed to produce bounded velocities. To see that, it is advantages to use the complex representation (2.2), in which solutions $u = x^n$ are described by

$$f(z) = \frac{z^{n+1}}{2}, \quad g(z) = \frac{z^n}{2}. \tag{2.22}$$

Indeed, the stream function is

$$\psi = \frac{1}{2} \Im\{z^{n+1} - \bar{z} z^n\} = y \Im\{i z^n\} = y x^n, \tag{2.23}$$

so we recover $u = \partial_y \psi = x^n$. Similarly, the streamfunction of a stokeslet (2.11) can be written $\psi = y \Re\{\ln z\}$.

Superimposing the solutions (2.23), we can write in general

$$\psi = y \Re\{\chi(z)\}, \text{ with } \chi(z) = d_0 \ln z + \sum_{n=0}^{\infty} d_{n+1} z^n. \tag{2.24}$$

By choosing

$$\chi(z) = -\frac{1}{2\pi} \ln \frac{8z}{r_c} + \frac{1}{4\pi} \sum_{n=1}^{\infty} (-1)^{n+1} \frac{e^{-4\pi n U} (8z)^{2n}}{r_c^{2n}} = \frac{1}{4\pi} \ln \left(e^{-4\pi U} + \frac{r_c^2}{(8z)^2} \right), \tag{2.25}$$

we have constructed a solution which for $z \to 0$ behaves like (2.12). On the other hand, for $z \to \infty$ we have $\chi \approx -U$, implying that a finite tangential velocity $u \approx -U$ is reached at infinity.

Looking at the behavior of χ in the complex plane, and using (2.17), one obtains

$$\chi = \frac{1}{4\pi} \ln \left(r_c^2 + \frac{r_c^2}{(8z)^2} \right) = \frac{1}{2\pi} \ln \frac{r_c}{8z} + \frac{1}{4\pi} \ln (z - i) + \frac{1}{4\pi} \ln (z + i), \tag{2.26}$$

which has logarithmic singularities at $z = \pm i$, or $y = \pm 1$. According to (2.24), this means that near the singularities

$$\psi = \pm \frac{1}{4\pi} \ln (z \mp i),$$

which are counter-rotating vortices of circulation $\Gamma = \mp 1/2$, situated at $z = \pm i$. This is very similar to the solution considered in Jeong (2010), where the flow leading to a cusp is driven by a pair of vortices. This, in turn, can be seen as an idealization of the experimental setups in Joseph *et al.* (1991) and Jeong & Moffatt (1992), where the flow is driven by two counter-propagating rollers.

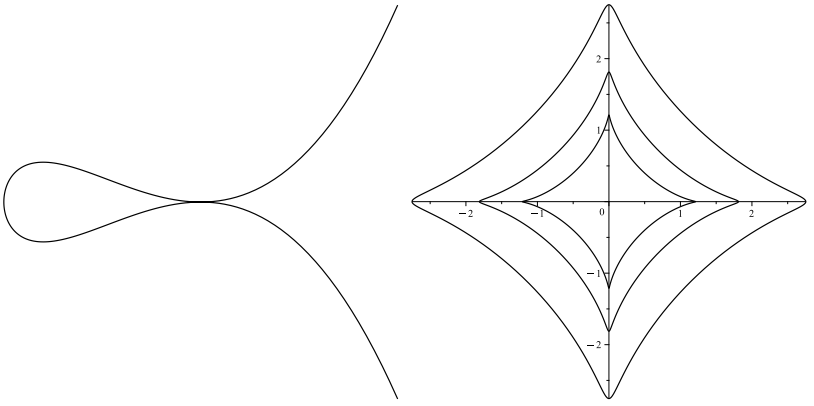

FIGURE 3. Left: A static solution to Stokes' equation, showing a bubble being enclosed at the tip of a cusp, as described by (3.3). The cusp opens like $h = x^{5/2}$. Right: A shrinking two-dimensional bubble, with a source of unit strength at the center, as described by (3.4) and (3.6) for $\hat{t} = 2, 1$, and 0.5; the bubble vanishes for $\hat{t} = 0$.

The particular solution considered in (2.25) is not universal, reflecting the fact that there are many different ways of driving a free surface to cusp formation. However, a universal feature of any such solution is the presence of singularities, of which the two vortices of (2.26) are a particular example. More generally, χ has to satisfy the requirement that $\chi \sim \ln z$ as $z \to 0$, to represent the stokeslet generated at the tip. This implies that $z\chi'(z) \sim 1$ as $z \to 0$: the combination $z\chi'(z)$ is free of singularities at the origin. In addition, the assumed boundedness of the velocity field at infinity implies that $z\chi'(z)$ can only grow sublinearly at infinity.

But supposing that $z\chi'(z)$ is analytic in the entire complex plane implies a contradiction: by Liouville's theorem, such an analytic function has to grow at least linearly at infinity, which would be inconsistent with the velocity remaining bounded. Thus the existence of singularities inside the flow, such as in (2.26), is a feature of the matching conditions we imposed. There is of course an infinite variety of ways such singularities can be imposed, corresponding to various ways in which the flow is driven.

3. Discussion

3.1. *Higher order singularities*

The remarkable property of the profile (2.16) is that it corresponds exactly to the generic singularity of a smooth, planar curve, which is being deformed smoothly to produce a self-intersection (Eggers & Fontelos 2015; Eggers & Suramlishvili 2017). At the critical point where intersection first occurs, the curve then produces a cusp $h \propto x^{3/2}$, but the tip remains rounded on a small scale in the neighborhood of that point. The generic behavior near such critical points is described by *singularity theory* (Arnol'd *et al.* 1993; Arnol'd *et al.* 1993), with the planar case described in more detail in Eggers & Suramlishvili (2017). Indeed, the symmetry of our problem under reflection suggests putting $x = s^2$, with s parameterizing the curve. Then (2.16) turns into the parameterized curve

$$(s^2, \sqrt{2r_c}s + cs^3). \tag{3.1}$$

Up to a rescaling of the axes, this corresponds to the *unfolding* of the germ (s^2, s^3) (Eggers & Suramlishvili 2017), the latter being the singular curve at the critical point.

Singularity theory demonstrates that up to smooth transformations, any deformation of the original germ can be written in the form $(s^2, \mu_1 s + s^3)$, where μ_1 is a parameter. But this exactly of the form (3.1), again up to trivial rescaling.

It is surprising that the terms appearing in (3.1) only involve integer powers, as required by singularity theory. This is a direct result of the fact that the stokeslet (2.11), although nominally the leading-order contribution to the velocity field, ends up making a subdominant contribution to the stress, as demonstrated by the estimate (2.20). As a result, logarithms do not appear in (2.13).

Thus it is natural to generalize (3.1) to unfoldings of higher order, corresponding to higher order terms in the sequence of powers appearing in (2.10) and (2.9). For example, if from the solutions $v = a_n x^{(2n-1)/2}$ one chooses $n = 2$, and from (2.9) one takes the leading order contribution $u = -U$, one obtains $h' = v/u = -(a_2/U)x^{3/2}$. After integration, we obtain $h = -2a_2/(5U)x^{5/2}$, and hence we have generated the so-called A_4 germ (s^2, s^5) (up to rescaling), discussed in detail in Eggers & Suramlishvili (2017). As this germ is of higher order, one obtains a more general class of unfoldings, which are

$$(s^2, \mu_1 s + \mu_3 s^3 + s^5), \tag{3.2}$$

with two parameters μ_1 and μ_3. But this is precisely the solution of Stokes' equation one obtains when including terms with for $n = 0, 1$, and 2 in the superposition (2.10).

In the generic case, in which $\mu_3 \neq 0$ has a finite value, the s^3 term will dominate over t^5 near the tip of the cusp, and we fall back onto the standard profile (2.16). However, if the external flow is fine-tuned so that μ_3 becomes small according to $\mu_3 = -2\sqrt{\mu_1}$ as $\mu_1 \to 0$, a bubble is formed, whose shape is described by

$$(x, y) = \left(s^2, s(s^2 - \sqrt{\mu_1})^2\right), \tag{3.3}$$

see Fig. 3, left. The cusp now opens like $h = x^{5/2}$, and the size of the bubble shrinks to zero as $\mu_1 \to 0$. Of course, other distinguished limits can be realized. A more detailed account of all the different possible structures is given in Fig. 6 of Eggers & Suramlishvili (2017).

3.2. *Time dependent solutions*

Our analysis can also be extended to cusps that evolve in time. Examples of such cusps are given by Tanveer & Vasconcelos (1994, 1995), who employed conformal mapping techniques to study cusp formation in contracting bubbles. They were able to derive exact solutions for a two-dimensional bubble driven by a point sink at its center. The simplest family of such solutions, corresponding to bubbles with $(N+1)$-fold symmetry, is shown on the right of Fig. 3 for $N = 3$. By taking the real and imaginary parts of Eqs. (84) together with (89) in Tanveer & Vasconcelos (1995), the solutions can be expressed in the parametric form

$$(x^*, y^*) = \sqrt{\frac{\mathcal{A}(t)}{\pi N(N\rho(t)^2 - 1)}}\,(N\rho(t)\cos\theta + \cos(N\theta), N\rho(t)\sin\theta - \sin(N\theta)), \tag{3.4}$$

where $-\pi \leqslant \theta < \pi$. Here (x^*, y^*). is measured from the bubble center, $\mathcal{A}(t)$ is the area of the bubble at time t, and $\rho(t)$ satisfies a nonlinear ODE, whose asymptotic solution is given below. As the bubble shrinks to zero, the size of the four tips decreases rapidly.

To find a local description near one of the tips, we expand (3.4) about $\theta = 0$, retaining

terms up to $O(\theta^3)$, resulting in

$$(x^*, y^*) \approx \sqrt{\frac{\mathcal{A}(t)}{\pi N(N\rho^2-1)}}\left(N\rho + 1 - \frac{N\rho+N^2}{2}\theta^2,\ (N\rho - N)\theta + \frac{N^3 - N\rho}{6}\theta^3\right). \quad (3.5)$$

If lengths are normalized so that the initial bubble area is π and the suction rate is chosen to be unity, $\mathcal{A}(t) = \pi - t$ and the bubble is fully depleted at $t_f = \pi$. Defining $\hat{t} = t_f - t\,(= \mathcal{A}(t))$, Tanveer & Vasconcelos (1995) expanded the exact solution as $\hat{t} \to 0$, showing that

$$\rho(t) \sim 1 + \exp\left(-\frac{2}{(N+1)\hat{t}^{1/2}}\sqrt{\frac{\pi N}{N-1}}\right) \quad (3.6)$$

(see Eqs. (89) and (97) of Tanveer & Vasconcelos (1995)). Substitution into the local expansion (3.5) yields

$$(x^*, y^*) \sim \sqrt{\tfrac{\hat{t}}{\pi N(N-1)}}\left(N+1-\tfrac{N+N^2}{2}\theta^2, N\exp\left(-\tfrac{2}{(N+1)\hat{t}^{1/2}}\sqrt{\tfrac{\pi N}{N-1}}\right)\theta + \tfrac{N^3-N}{6}\theta^3\right), \quad (3.7)$$

where, in each monomial in θ, only the dominant term in $\hat{t}$ has been kept.

Upon shifting the axes such that the right-hand cusp tip is at the origin, rescaling the axes, and absorbing the time-independent factor $\frac{1}{8(N+1)}\sqrt{\frac{N}{\pi(N-1)}}$ into the lengthscale, (3.7) can be recast in the form (2.16), with

$$h = 4\hat{t}^{1/4}\exp\left(-\frac{2}{N+1}\sqrt{\frac{\pi N}{N-1}}\hat{t}^{-1/2}\right)x^{1/2} + \frac{1}{6}\frac{N-1}{N+1}\hat{t}^{-1/4}x^{3/2}. \quad (3.8)$$

The coefficient of the $x^{1/2}$ term, corresponding to $\sqrt{2r_c}$ in (2.16), goes to zero exponentially fast as $\hat{t} \to 0$, thus demonstrating the approach to a singular cusp, as illustrated in Fig. 3.

The profile (3.8) can be understood in the light of the local description of §2.2. First, since the area of the bubble decreases linearly in $\hat{t}$, the natural lengthscale for the size of the bubble (the outer region) is $L \propto \hat{t}^{1/2}$. To remove this implicit time dependence, we rescale the local variables as $h \mapsto \hat{t}^{1/2}h$ and $x \mapsto \hat{t}^{1/2}x$, such that (2.16) becomes

$$h = \sqrt{2r_c}\hat{t}^{1/4}x^{1/2} + c\hat{t}^{-1/4}x^{3/2}. \quad (3.9)$$

Furthermore, since the outer flow is driven by a point sink, velocities scale as $1/L \propto \hat{t}^{-1/2}$. To account for this, we rescale the velocity field according to $(u, v) \mapsto \hat{t}^{-1/2}(u, v)$. With this rescaling, (2.17) gives $r_c = 8\exp\left(-2\pi U\hat{t}^{-1/2}\right)$, where U is independent of time. Substituting r_c into (3.9) yields

$$h = 4\hat{t}^{1/4}\exp\left(-\pi U\hat{t}^{-1/2}\right)x^{1/2} + c\hat{t}^{-1/4}x^{3/2}, \quad (3.10)$$

which agrees with (3.8). Note that while the determination U and c requires the solution of the outer problem (or comparison with (3.8)), the asymptotic description captures both the geometry and temporal evolution of the cusp.

This shows that our analysis extends naturally to unsteady problems, provided the coefficients are allowed to vary in time. To properly justify that, note that unsteadiness enters only through the kinematic boundary condition, which for small slopes reads $h_t = v - uh'$. For the time-dependent cusps discussed above, we have $h_t = O(h/\hat{t})$ and $uh' = O\left(h/(\hat{t}^{1/2}\sqrt{r_c})\right)$. In the latter expression, we used that the velocity scales as $\hat{t}^{-1/2}$ and that the cusp lengthscale is $\sqrt{r_c}$, as shown in §2.2. Since r_c is exponentially small

in $\hat{t}$, the advective term uh' dominates h_t, hence the leading-order balance reduces to $v = uh'$, and the cusp dynamics is therefore *quasi-steady*. In view of this, we expect the same framework to describe other types of time-dependent cusps, such as those in Fig. 5 of Tanveer & Vasconcelos (1995), where a small bubble is enclosed at the tip, which appears to be analogous to the cusp on the left of Fig. 3.3.

Finally, another generalization is to consider departures from exactly two-dimensional flow: this is easily built in by allowing μ_1 to be a function of a third variable z. As long as this variation takes place on a scale much smaller than the tip curvature, the above asymptotics will remain valid, and will describe a three-dimensional flow to leading order.

Acknowledgments

M. A. F. acknowledges financial support through projects PID2022-139524NB-I00 and PID2023-150166NB-I00.

Declaration of interests

The authors report no conflict of interest.

REFERENCES

Antanovskii, L. K. 1996 Formation of a pointed drop in taylor's four-roller mill. *J. Fluid Mech.* **327**, 325.

Arnol'd, V. I., Vasil'ev, V. A., Goryunov, V. V. & Lyashko, O. V. 1993 Singularity theory I: local and global theory. In *Dynamical Systems VI*. Heidelberg: Springer.

Arnol'd, V. I., Vasil'ev, V. A., Goryunov, V. V. & Lyashko, O. V. 1993 Singularity theory II: Classification and applications. In *Dynamical Syatems VIII*. Heidelberg: Springer.

Crowdy, D. 2002 Exact solutions for two steady inviscid bubbles in the slow viscous flow generated by a four-roller mill. *J. Engin. Math.* **44**, 311.

Cummings, L. J. 2000 Steady solutions for bubbles in dipole-driven Stokes flows. *Phys. Fluids* **12**, 2162.

Cummings, L. J. & Howison, S. D. 1999 Two-dimensional Stokes flow with suction and small surface tension. *Euro. J. Appl. Math.* **10**, 681–706.

Eggers, J. 2001 Air entrainment through free-surface cusps. *Phys. Rev. Lett.* **86**, 4290–4293.

Eggers, J. 2023 Viscous free surface cusps - local solution. *Phys. Rev. Fluids* **8**, 124001.

Eggers, J. & Fontelos, M. A. 2015 *Singularities: Formation, Structure, and Propagation*. Cambridge University Press, Cambridge.

Eggers, J. & Suramlishvili, N. 2017 Singularity theory of plane curves and its applications. *Eur. J. Mech. B* **65**, 107–131.

Gillow, K. 1998 Codimension-two free boundary problems. PhD thesis, Oxford University.

Hopper, R. W. 1993 Capillarity-driven plane Stokes flow exterior to a parabola. *Q. J. Mech. appl. Math.* **46**, 193.

Howison, S. D., Morgan, J. D. & Ockendon, J. R. 1997 A class of codimension-two free boundary problems. *SIAM Rev.* **39**, 221–253.

Jeong, J.-T. 1999 Formation of cusp on the free surface at low Reynolds number flow. *Phys. Fluids* **11**, 521.

Jeong, J.-T. 2007 Free surface deformation due to a source or sink in Stokes flow. *Eur. J. Mech. B/Fluids* **26**, 720.

Jeong, J.-T. 2010 Two-dimensional Stokes flow due to a pair of vortices below the free surface. *Phys. Fluids* **22**, 082102.

Jeong, J.-T. & Moffatt, H. K. 1992 Free-surface cusps associated with a flow at low Reynolds numbers. *J. Fluid Mech.* **241**, 1–22.

Joseph, D. D., Nelson, J., Renardy, M. & Renardy, Y. 1991 Two-dimensional cusped interfaces. *J. Fluid Mech.* **223**, 383–409.

Kiger, K. T. & Duncan, J. H. 2012 Air-entrainment mechanisms in plunging jets and breaking waves. *Annu. Rev. Fluid Mech.* **44**, 563–596.

Lorenceau, E., Quéré, D. & Eggers, J. 2004 Air entrainment by a viscous jet plunging into a bath. *Phys. Rev. Lett.* **93**, 254501.

Lorenceau, É., Restagno, F. & Quéré, D. 2003 Fracture of a viscous liquid. *Phys. Rev. Lett.* **90**, 184501.

Morgan, J. D. 1994 Codimension-two free boundary problems. PhD thesis, Oxford University.

Pozrikidis, C. 1992 *Boundary Integral and singularity methods for linearized flow*. Cambridge University Press, Cambridge.

Richardson, S. 1968 Two-dimensional bubbles in slow viscous flows. *J. Fluid Mech.* **33**, 476.

Tanveer, S. & Vasconcelos, G. L. 1994 Bubble breakup in two-dimensional Stokes flow. *Phys. Rev. Lett.* **73** (21), 2845.

Tanveer, S. & Vasconcelos, G. L. 1995 Time-evolving bubbles in two-dimensional Stokes flow. *J. Fluid Mech.* **301**, 325.